Korean J. Chem. Eng., 39(7), 1831-1838 (2022)
DOI: 10.1007/s11814-021-1034-7

pISSN: 0256-1115
eISSN: 1975-7220

Polymerization mechanism of polyferric aluminum phosphatic sulfate (PFAPS) and its flocculation effect on simulated dye wastewater

Shaopu Li and Yong Kang†

School of Chemical Engineering and Technology, Tianjin University, Tianjin 300350, China
(*Received 25 September 2021 • Revised 29 November 2021 • Accepted 2 December 2021*)

Abstract−Inorganic polymer flocculants play an important role in water treatment. The copolymerization of Al^{3+} and Fe^{3+} in proportion can prepare polyferric aluminum (PFA), which can improve the flocculation performance of polyferric (PFe) on the premise of reducing Al^{3+} residue. The effects of Al/Fe and OH^-/Fe on the micromorphology, physicochemical properties and flocculation performance of polyferric aluminum phosphatic sulfate (PFAPS) were studied in this work. The results show that Fe^{3+} and Al^{3+} form Fe-monomer and Al-monomer by combining with six oxygen atoms from H_2O or anion. And then these monomers form polymers through the bridging of various anions. Although the binding mode is similar, XRD results show that pfaps and PFPS are amorphous. The flocculation performance of PFAPS first increases and then decreases with the increase of Al/Fe and OH^-/Fe.

Keywords: Polymerization Mechanism, Simulated Dye Wastewater, Molecular Dynamics Simulation

INTRODUCTION

The security of water resources plays a crucial role in the sustainable development of human society, what is the basic resource of promoting economic development and social progress [1]. Environmentally-safe treatment of domestic and industrial wastewater containing pollutants, on the one hand, can avoid polluting more water sources; on the other hand, can also recycle the treated water [2]. Flocculation-coagulation is one of the most widely applied wastewater treatment technologies [3]. With the continuous development of flocculants, flocculation can not only separate suspended solids from water [4], but also play a role in oil removal [5], decolorization [6], phosphorus removal [7], heavy metal removal [8], and organic matter removal [9] of water treatment.

Polyaluminum (PAl) is one of the most frequently used flocculants [10,11]. Compare with metal salts such as $AlCl_3$ or $Al_2(SO_4)_3$, whose morphology distribution of the formed metal ion polymer cannot be controlled due to its rapid hydrolysis in the wastewater [12], PAl has better flocculant performance. PAl contain many positively charged polymers. They can destabilize the colloidal pollutants by electric neutralization and compressing electric double layer, and form flocs which are easy to precipitate by adsorption bridging and net sweeping [13].

However, Al can cause oxidative stress and inflammation in human body, damage multiple organs [14], destroy intestinal barrier [15] and brain nerve cells [16]. In 1989, the World Health Organization (WHO) and the Food and Agriculture Organization (FAO) of the United Nations officially listed Al as a food pollutant. While Fe is basically harmless to human body, and Ployferric (PFe) has the advantages of wide raw material sources, low production cost, non-toxic, wide temperature and pH value application range [17-19], what is an ideal substitute for PAl. However, the flocculation performance and stability of PFe are weaker than of PAl. Composite flocculant polyferric aluminum (PFA) is formed by copolymerization of Al^{3+} and Fe^{3+} in proportion, which can reduce the residual of Al and improve the flocculation performance of PFe. Although PFA has been reported that it has good flocculation effect on turbidity and COD [20-23], it also has a broader application prospect in the treatment of chemical engineering, paper, dye, mining and other industry wastewater and a certain research value in its polymerization mechanism. The understanding of its polymerization mechanism is not only conducive to the determination of its optimal preparation conditions, but also conducive to its utilization in wastewater treatment.

In this paper, polyferric aluminum phosphatic sulfate (PFAPS) was prepared by copolymerization of $Fe_2(SO_4)_3$ and $Al_2(SO_4)_3$ with $FeSO_4{\cdot}7H_2O$ and $Al_2(SO_4)_3{\cdot}18H_2O$ as raw materials, H_2O_2 as oxidant and H_3PO_4 as stabilizer. The effects of Al/Fe and OH^-/Fe on the polymerization and flocculation performance of PFAPS were studied. The crystal structure and chemical bond of PFAPS were characterized by XRD and FTIR. And the polymerization mechanism of PFAPS was studied by molecular dynamics (MD) simulation.

EXPERIMENTAL

1. MD Simulation Details

In this work, GROMACS 2018.4 software package [24] was used to simulate the PFPS, $PFAPS_3$ and $PFAPS_8$. According to the molar ratio of ions in the actual preparation system, considering the local aggregation of OH^- around Fe^{3+} and Al^{3+}, the particle number are determined. There are 2000 H_2O, 48 OH^-, 24 SO_4^{2-}, 16 PO_4^{3-} and 48 Fe^{3+} in PFPS system. There are 2000 H_2O, 48 OH^-, 33 SO_4^{2-}, 18 PO_4^{3-}, 48 Fe^{3+} and 8 Al^{3+} in $PFAPS_3$ system. There are 2000 H_2O, 56 OH^-, 28 SO_4^{2-}, 18 PO_4^{3-}, 48 Fe^{3+} and 8 Al^{3+} in $PFAPS_8$ system.

†To whom correspondence should be addressed.
E-mail: ykang@tju.edu.cn

The initial structures of H_2O, OH^-, SO_4^{2-} and PO_4^{3-} were constructed by Guassview6 and optimized by Gaussian 09 using B3LYP theory and 6-311G+(3df2) basis set. The restrained electrostatic potential (RESP) of the atom was calculated by Multiwfn 3.8 [25]. The force field (GAFF) in AMBER [26] was used to obtain the force field parameters of each particle except Fe^{3+} and Al^{3+}. The force fields of Fe^{3+} and Al^{3+} were obtained from reference [27]. TIP3P water model was used in the simulation.

Packmol [28] was used to arrange the particles of the simulation systems in 7×7×7 nm simulation box with periodic boundary, and the distance between the molecules is more than 0.2 nm. The energy minimization method was used to optimize the simulation box, and the maximum force between atoms was less than 500 kJ/(mol·nm). At a constant temperature (298.15 K) and a constant pressure (1 bar), V-rescale and Parrinello Rahman methods were used to control the temperature and pressure, respectively. The NVT ensemble of 100 ps was carried out with step size of 2 fs. After the temperature equilibrium was reached, the NPT ensemble of 100 ps was carried out with step size of 2 fs. Then, under isothermal and isobaric conditions, the MD simulation with step size of 0.8 fs was carried out for 50 ns to obtain the final simulation results.

2. Materials

$FeSO_4·7H_2O$ (Tianjin kermel Co., China), H_2O_2 (Tianjin Chemical Reagent Supply and Marketing Co., China), $Al_2(SO_4)_3·18H_2O$ (Tianjin Damao Co., China), H_2SO_4 (Tianjin Damao Co., China) and Na_2CO_3 (Tianjin Jiangtian Co., China) used in this study are analytical grade reagents. Except for simulated wastewater, the solvents used are deionized water (the conductivity 2.55 μS/cm, Tianjin Yongqingyuan Co., China).

3. Preparation of PFPS and PFAPS

0.05 mol $FeSO_4·7H_2O$ and 0.005 mol H_2SO_4 were added in 10 ml deionized water, and then they were stirred to mix evenly in a water bath at 30 °C. Under stirring condition, 0.04 mol H_2O_2 was dripped into solution for oxidation. After 30 min, it was placed at room temperature. 0.005 mol H_3PO_4 was added and stirred for 10 min. $Al_2(SO_4)_3·18H_2O$ was added according to different Al/Fe ratios and stirred for 10 min. And then liquid PFAPS samples with different Al/Fe ratios were obtained by aging in water bath at 50 °C for 2 h. To obtain PFAPS samples with different OH^-/Fe, after adding $Al_2(SO_4)_3·18H_2O$ according to Al/Fe=0.15, Na_2CO_3 was added according to different OH^-/Fe and stirred for 10 min. PFAPS samples with different OH^-/Fe were obtained by aging in 50 °C water bath for 2 h. The specific preparation parameters are shown in Table 1.

Table 1. Preparation parameters of PFS and $PFAPS_x$

No	Al/Fe	OH^-/Fe
PFPS	0	0
$PFAPS_1$	0.05	0
$PFAPS_2$	0.1	0
$PFAPS_3$	0.15	0
$PFAPS_4$	0.2	0
$PFAPS_5$	0.15	0.025
$PFAPS_6$	0.15	0.05
$PFAPS_7$	0.15	0.1
$PFAPS_8$	0.15	0.2
$PFAPS_9$	0.15	0.3

4. Analytical Methods for PFAPS

The content of Fe^{2+}([Fe^{2+}]), The content of total Fe ([TFe]) and OH^-/(Al+Fe) of PFAPS were determined according to GB/T14591-2016 *Water treatment chemicals—Poly ferric sulfate* [29]. According to the method described in the literature [30], Ferron-Fe timed spectroscopy method was used to determine the distribution of Fe(III) species. According to the different reaction time with Ferron, Fe(III) can be divided into Fe_a, Fe_b and Fe_c species. Fe_a is the component that reacts with Ferron in 30 seconds, what is considered to be Fe^{3+} and Fe-monomer, Fe_b is the component that reacts with Ferron in 30 seconds to 24 hours, what is considered to be Fe-polymer. And Fe_c is the component that still does not react with Ferron in 24 hours, what is considered to be uncharged precipitate. The conductivity of the liquid PFAPS samples was measured by conductivity meter (DDSJ-318, Shanghai INESA Scientific Instrument, China). Some liquid samples were dried at 70 °C for 24 h to prepare solid PFAPS for XRD (MiniFlex600, Rigaku, Japan, scanning rate: 4°/min, radiation range: 10°-80° (2θ)) and FTIR (Nicolet 6700, Thermo Fisher Scientific, USA, spectral range: 4,000-400 cm^{-1}) characterizations.

5. Simulated Dye Wastewater

Disperse yellow (DY, Zhejiang Shanyu Dyestuff Co., China) and reactive turquoise blue (RTB, Shanghai Wande Co., China) were used for the flocculation experiments of PFAPS. DY is a hydrophobic dye, and RTB is an anionic hydrophilic dye. Tap water was used to prepare these dyes into 0.1 g/L simulated dye wastewater for assessing the flocculation performance of PFAPS. The absorbance at 445 nm and 618 nm is proportional to the concentration of DY and RTB simulated dye wastewater respectively. And the absorbance of 0.1 g/L DY and RTB simulated dye wastewater are 1.0165±0.027 Abs and 1.4611±0.019 Abs respectively.

6. Flocculation Experiments

Flocculation experiment was carried out at 25 °C on the coagulation test mixer (MY3000-6M, Wuhan Meiyu Co. Ltd., China). In each experiment, 200 ml dye solution in a 300 ml beaker was added liquid PFAPS with a certain dosage and stirred at 250 rpm for 1 min, then at 35 rpm for 15 min, and the flocculated dye solution stood for 20 min. The above supernatant was sampled for measuring the pH value by a pH meter (PHS-3C, Shanghai Youke Instrument Co., China, Measuring range: 0-14.00 pH, Basic error: ±0.02 pH). The supernatant absorbance was determined by an ultraviolet visible spectrophotometer (L6S, Shanghai Precision Instrument Co., China, Wavelength range: 190-1,100 nm, Absorbance range: –0.301-4.000 A, Maximum allowable error: ±0.3%), and the decolorization efficiency of the dye solution was calculated according to Eq. (1). The residual PO_4^{3-} and Al^{3+} of DY and RTB supernatant treated by $PFAPS_{1\text{-}9}$ in experimental maximum dose are measured by multiparameter Water Survey Instrument (HI 83200, Hanna Instruments, Inc., Italy).

$$\text{Decolorization efficiency}\ (\%) = \frac{A_0 - A_1}{A_0} \times 100\% \quad (1)$$

where A_0 and A_1 is the absorbance of the dye solution and the super-

natant of the flocculated the dye solution, respectively.

RESULTS AND DISCUSSION

1. MD Simulation Results

The molecular dynamics (MD) simulation results of PFPS, $PFAPS_3$ and $PFAPS_8$ are shown in Fig. 1, and the results of MD simulation without H_2O which is not bound with Fe^{3+} are shown in Fig. 2.

As shown in Fig. 2, the surrounding of Fe^{3+} and Al^{3+} will be regularly arranged with six oxygen atoms from the same or different particles to form Fe-monomer and Al-monomer. This is because Fe^{3+} and Al^{3+} both have 1 s orbital, 3 p orbitals and 2 d orbitals hybridized into sp^3d^2 orbitals which contain lone pair electrons of the surrounding six oxygen atoms to form ligands. These Fe-monomers and Al-monomers are the raw material of polynuclear complex ion (polymers) production in polymerization process of Fe based and Al based inorganic polymer flocculants [31-34]. Different kinds of Fe-monomers and Al-monomers in the three systems are shown in Fig. S1 and Fig. S2, respectively. There are 3 $[Fe(H_2O)_6]^{3+}$ (Fig. S1(a)), 15 $[Fe(H_2O)_5OH]^{2+}$ (Fig. S1(b)), 4 $Fe(H_2O)_5SO_4]^+$ (Fig. S1(c)), 4 $Fe(H_2O)_5PO_4$ (Fig. S1(d)), 1 $[Fe(H_2O)_4(OH)_2]^+$ (Fig. S1(e)), 4 $Fe(H_2O)_4OHSO_4$ (Fig. S1(f)), 2 $[Fe(H_2O)_4OHPO_4]^-$ (Fig. S1(g)), 2 $Fe(H_2O)_4PO_4$ (Fig. S1(j)), 2 $Fe(H_2O)_3(PO_4)_2$ (Fig. S1(k)), 1 $[Fe(H_2O)_3PO_4SO_4]^{2-}$ (Fig. S1(m)), 2 $[Fe(H_2O)_3PO_4SO_4]^{2-}$ (Fig. S1(n)), 4 $Fe(H_2O)_3OHSO_4$ (Fig. S1(p)), 1 $[Fe(H_2O)_3OHPO_4]^-$ (Fig. S1(q)), 1 $[FeH_2O(SO_4)_2PO_4]^{4-}$ (Fig. S1(s)), 1 $[Fe(H_2O)_2(PO_4)_2]^{3-}$ (Fig. S1(u)) and 1 $[Fe(H_2O)_2(SO_4)_2PO_4]^{4-}$ (Fig. S1(v)) in the PFPS simulation system; There are 2 $[Fe(H_2O)_6]^{3+}$ (Fig. S1(a)), 18 $[Fe(H_2O)_5OH]^{2+}$ (Fig. S1(b)), 5 $[Fe(H_2O)_5SO_4]^+$ (Fig. S1(c)), 8 $Fe(H_2O)_5PO_4$ (Fig. S1(d)), 2 $[Fe(H_2O)_4(OH)_2]^+$ (Fig. S1(e)), 4 $[Fe(H_2O)_4OHPO_4]^-$ (Fig. S1(g)), 1 $[Fe(H_2O)_4(PO_4)_2]^{3-}$ (Fig. S1(h)), 1 $[Fe(H_2O)_4SO_4PO_4]^{2-}$ (Fig. S1(i)), 2 $Fe(H_2O)_4PO_4$ (Fig. S1(j)), 1 $[Fe(H_2O)_3PO_4SO_4]^{2-}$ (Fig. S1(n)), 1 $Fe(H_2O)_3OHSO_4$ (Fig. S1(p)), 2 $[Fe(H_2O)_3OHPO_4]^-$ (Fig. S1(q)), 1 $[FeH_2OOHPO_4SO_4]^{3-}$ (Fig. S1(t)), 4 $[Al(H_2O)_6]^{3+}$ (Fig. S2(a)), 1 $[Al(H_2O)_5OH]^{2+}$ (Fig. S2(b)), 2 $Al(H_2O)_4PO_4$ (Fig. S2(c)) and 1 $[AlH_2O(SO_4)_3]^{3-}$ (Fig. S2(h)) in the $PFAPS_3$ simulation system; There are 4 $[Fe(H_2O)_6]^{3+}$ (Fig. S1(a)), 16 $[Fe(H_2O)_5OH]^{2+}$ (Fig. S1(b)), 5 $[Fe(H_2O)_5SO_4]^+$ (Fig. S1(c)), 1 $Fe(H_2O)_5PO_4$ (Fig. S1(d)), 5 $[Fe(H_2O)_4(OH)_2]^+$ (Fig. S1(e)), 1 $Fe(H_2O)_4OHSO_4$ (Fig. S1(f)), 1 $[Fe(H_2O)_4OH\ PO_4]^-$ (Fig. S1(g)), 1 $Fe(H_2O)_4PO_4SO_4$ (Fig. S1(i)), 4 $Fe(H_2O)_4PO_4$ (Fig. S1(j)), 1 $Fe(H_2O)_3(PO_4)_2$ (Fig. S1(k)), 1 $[Fe(H_2O)_3PO_4SO_4]^{2-}$ (Fig. S1(m)), 1 $[Fe(H_2O)_3$

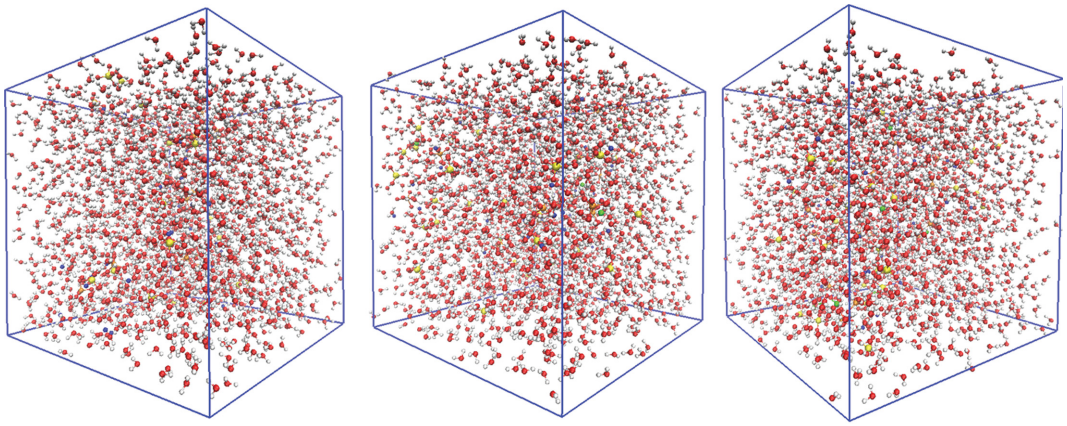

(a) (b) (c)

Fig. 1. The MD simulation results of the simulation systems of PFPS (a) $PFAPS_3$ (b) and $PFAPS_8$ (c) (Red: O, White: H, Yellow: S, Blue: Fe, Orange: P, Green: Al).

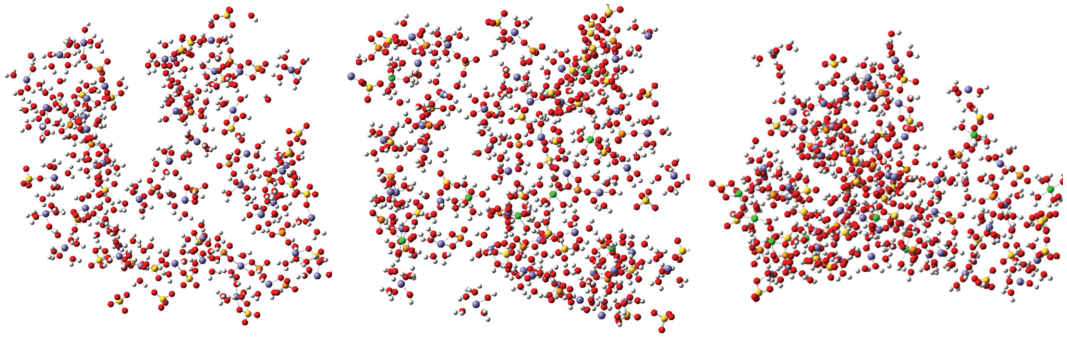

(a) (b) (c)

Fig. 2. The MD simulation results without H_2O which not bound with Fe^{3+} of PFPS (a) $PFAPS_3$ (b) and $PFAPS_8$ (c) simulation systems (Red: O, White: H, Yellow: S, Blue: Fe, Orange: P, Green: Al).

$PO_4SO_4]^{2-}$ (Fig. S1(n)), 2 $Fe(H_2O)_3OHSO_4$ (Fig. S1(p)), 1 $[Fe(H_2O)_3OHPO_4]^-$ (Fig. S1(q)), 1 $[Fe(H_2O)_2(OH)_2PO_4]^{2-}$ (Fig. S1(r)), 1 $[Fe(H_2O)_2(SO_4)_2PO_4]^{4-}$ (Fig. S1(w)), 1 $[FeH_2OSO_4(PO_4)_2]^{5-}$ (Fig. S1(x)), 1 $[Fe(H_2O)_2OH\ (PO_4)_2]^{4-}$ (Fig. S1(y)), 2 $[Al(H_2O)_6]^{3+}$ (Fig. S2(a)), 1 $Al(H_2O)_4PO_4$ (Fig. S2(c)), 1 $[Al(H_2O)_3OHPO_4]^-$ (Fig. S2(d)), 1 $Al(H_2O)_4OHSO_4$ (Fig. S2(e)), 1 $[Al(H_2O)_3PO_4SO_4]^{2-}$ (Fig. S2(f)) and 2 $[Al(H_2O)_3SO_4]^+$ (Fig. S2(g)) in the $PFAPS_8$ simulation system.

According to the MD simulation results shown in Fig. 2, compared the results of PFPS and $PFAPS_3$, the addition of Al^{3+} will affect the number of anions bound with Fe^{3+}, and then affect the polymerization of Fe-polymer. Specifically, the number of PO_4^{3-} bound with Fe^{3+} decreases from 15 to 12, while the number of OH^- bound with Fe^{3+} increases from 28 to 31. It indicates that the addition of Al^{3+} will compete with Fe^{3+} for PO_4^{3-}, which is adverse to the substitution of PO_4^{3-} for OH^- in Fe^{3+} polymerization and promotes the hydrolysis of Fe^{3+}. Comparing the results of $PFAPS_3$ and $PFAPS_8$, the addition of OH^- can promote the polymerization of both Al^{3+} and Fe^{3+}. Specifically, the number of OH^- bound with Fe^{3+} increases from 31 to 35, and the number of OH^- bound with Al^{3+} increases from 1 to 4.

Fe-monomers and Al-monomers form polymers through the bridging of various anions [31-34], such as OH^-, PO_4^{3-}, and SO_4^{2-}. According to the MD simulation results shown in Fig. 2, the metal ion monomers formed with Al^{3+} and Fe^{3+} as the center will form micro polymers by the bridging of anions in three forms: (1) different monomers share the same anion, (2) The mutual attraction between different monomers, and (3) different monomers are attracted by the same anion, as shown in Fig. S3. In the three simulation systems of PFPS, PFAPS3 and $PFAPS_8$, the micro-polymer formed in mode (1) is shown in Fig. S3((a), (b) and (c)); The micro-polymer formed in mode (2) is shown in Fig. S3((d), (e), (f)); The micro-polymer formed in mode (3) is shown in Fig. S3((g), (h), (j)). These micro polymers will continue to form larger polymers through the latter two ways.

2. Characterization of PFAPS

2-1. Physicochemical Properties of PFAPS

(1) Effect of Al/Fe

The physicochemical properties of PFAPS samples with different Al/Fe ratios are shown in Table 2. The results show that with the increase of Al/Fe, the density of flocculant samples increases, the [TFe] and OH^-/3(Fe+Al) of PFAPS samples decreases, and its pH value changes little. The conductivity of $PFAPS_1$, $PFAPS_2$ and $PFAPS_3$ are similar, lightly higher than that of PFPS, and significantly lower than that of $PFAPS_4$. It shows that when Al/Fe>0.15, the newly added Al^{3+} no longer combines with the existing charged particles, but forms new charged particles, which makes the conductivity of the sample increase obviously. The $[Fe^{2+}]$ of PFPS samples is lower than 0.01%, which indicates that Fe^{2+} is completely oxidized during the preparation process. The results of Fe(III) species distribution show that compared with PFPS, the content of Fe_a increases, the content of Fe_c decreases, while the content of Fe_b changes little in $PFAPS_1$. This is because the addition of Al^{3+} will compete with Fe^{3+} for OH^-, hinder the combination of Fe^{3+} and OH^-, and affect the polymerization of Fe polymer, resulting in the increase of Fe_a and the decrease of Fe_c. Then, with the increase of Al/Fe, the content of Fe_a changes little, the content of Fe_b slightly decreases and the content of Fe_c slightly increases. This is because that the addition of Al^{3+} will compete with Fe^{3+} for PO_4^{3-}, which is adverse to the substitution of PO_4^{3-} for OH^- in the polymerization process of Fe^{3+}, resulting in the reduction of the stability of Fe-polymer and the improvement of the content of uncharged precipitation.

(2) Effect of OH^-/Fe

The physicochemical properties of PFAPS samples with different OH^-/Fe are shown in Table 3. The results show that with the increase of OH^-/Fe, the density and [TFe] of PFPS samples decrease,

Table 2. Characteristics of flocclant samples with different Al/Fe ratios

No	Al/Fe (mol/mol)	Density (g/ml)	$[Fe^{2+}]$ (wt%)	[TFe] (wt%)	pH	Conductivity (mS/cm)	OH^-/ 3(Fe+Al)	Fe(III) species (%)		
								Fe_a	Fe_b	Fe_c
PFPS	0	1.244	0.0056	7.60	1.44	17.04	0.217	74.6	15.3	10.1
$PFAPS_1$	0.05	1.290	0.0067	7.63	1.43	17.35	0.173	81.4	15.7	3.0
$PFAPS_2$	0.1	1.306	0.0061	7.59	1.43	17.40	0.175	80.9	14.4	4.8
$PFAPS_3$	0.15	1.329	0.0056	7.54	1.47	17.45	0.170	80.1	14.0	5.8
$PFAPS_4$	0.2	1.335	0.0067	7.24	1.47	18.77	0.164	79.7	13.8	6.5

Table 3, Characteristics of PFPS samples with different OH^-/Fe ratios

No	OH^-/Fe (mol/mol)	Density (g/ml)	$[Fe^{2+}]$ (wt%)	[TFe] (wt%)	pH	Conductivity (mS/cm)	OH^-/ 3(Fe+Al)	Fe(III) species (%)		
								Fe_a	Fe_b	Fe_c
$PFAPS_3$	0	1.33	0.0056	7.5	1.47	17.45	0.170	80.1	14.0	5.8
$PFAPS_5$	0.025	1.32	0.0056	7.2	1.53	19.05	0.172	76.0	17.9	6.1
$PFAPS_6$	0.05	1.30	0.0056	7.2	1.56	19.50	0.174	75.7	17.2	7.2
$PFAPS_7$	0.1	1.30	0.0056	7.0	1.66	19.90	0.219	75.7	15.7	8.6
$PFAPS_8$	0.2	1.29	0.0067	7.1	1.92	20.80	0.237	75.3	13.0	11.7
$PFAPS_9$	0.3	1.28	0.0056	7.0	1.99	22.40	0.238	73.8	10.6	15.6

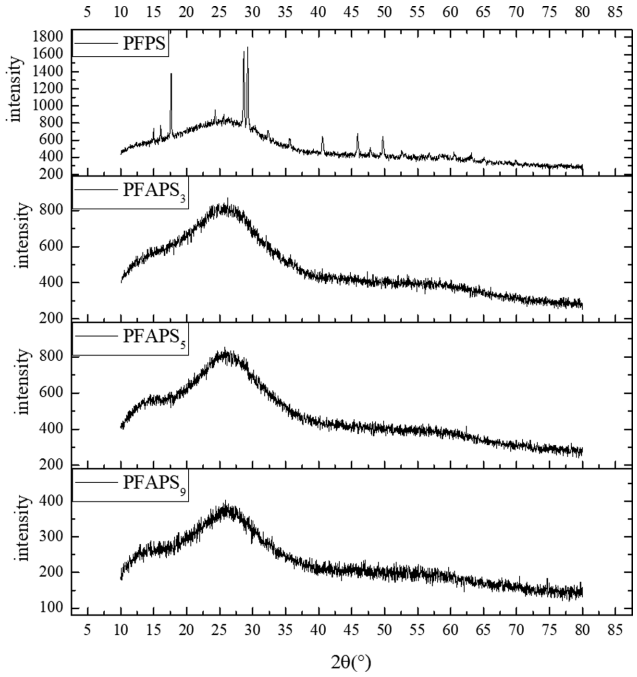

Fig. 3. XRD results of the powder samples of PFPS, $PFAPS_3$, $PFAPS_5$ and $PFAPS_9$.

while the pH value, conductivity and $OH^-/3(Fe+Al)$ increase. The $[Fe^{2+}]$ of PFPS samples is lower than 0.01%, which indicates that Fe^{2+} is completely oxidized during the preparation process. The results of Fe(III) species distribution show that compared with $PFAPS_3$, the content of Fe_a decreases, the content of Fe_b and Fe_c increase in $PFAPS_5$. Then, with the increase of OH^-/Fe, the content of Fe_a changes little, the content of Fe_b slightly decreases and the content of Fe_c slightly increases. This is due to the reaction of Na_2CO_3 with H^+ in the preparation solution, which increases the concentration of OH^-, and promotes the polymerization of Fe polymer. When $OH^-/Fe<0.025$, Fe_a can be promoted to polymerize into Fe_b, and then addition more Na_2CO_3 can promote Fe_b to polymerize into Fe_c. At the same time, the increase of OH^-/Fe can also promote the polymerization of Al-polymer.

2-2. XRD Results

Liquid samples of PFPS, $PFAPS_3$, $PFAPS_5$ and $PFAPS_9$ were dried at 70 °C for 24 h and then ground to obtain solid powder samples which were characterized by XRD. The results are shown in Fig. 3, which indicate that PFPS, $PFAPS_3$, $PFAPS_5$ and $PFAPS_9$ are amorphous structure. The results show that the addition of Al^{3+} does not produce crystal PFAPS. Although the increase of OH^-/Fe can promote the polymerization of PFAPS and improve its crystallinity, it is still unable to form a three-dimensional periodic crystal structure. These results are similar to the XRD results of inorganic polymer flocculants in the literature [13].

2-3. FTIR Results

Liquid samples of PFPS, $PFAPS_3$ and $PFAPS_9$ were dried at 70 °C for 24 h and then ground to obtain solid powder samples which were characterized by FTIR. The results are shown in Fig. 4. The broad absorption peak at 3,100-3,400 cm^{-1} corresponds to the stretching vibration of -OH [35], the absorption peak near 3,180 cm^{-1} corresponds to the OH group bound with Fe [36], and the absorption peak near 3,370 cm^{-1} corresponds to the OH group bound with Al [37]. The comparison shows that the addition of Al^{3+} makes Al-OH appear in $PFAPS_3$, and the increase of OH^-/Fe enhances the existence of Al-OH in $PFAPS_9$. Three samples all have absorption peaks near 1,645 cm^{-1}, corresponding to the bending vibration of H-O-H [38], indicating the presence of bound water in the samples. The absorption peak near 1,100 cm^{-1} corresponds to Fe-OH-Fe [39] or Al-OH-Al group [33], while the absorption peak near 1,035 cm^{-1} corresponds to Fe-O-P [40]. It is found that both PFPS and $PFAPS_9$ have absorption peaks near 1,100 cm^{-1} and 1,035 cm^{-1}, while $PFAPS_3$ only has absorption peak near 1,100 cm^{-1}. This is because that the addition of Al^{3+} make Al-OH-Al which enhances the absorption peaks near 1,100 cm^{-1} produce in the sample, While the competition between Al^{3+} and Fe^{3+} for PO_4^{3-} weakens the absorption peak near 1,035 cm^{-1}; The increase of OH^- concentration in $PFAPS_9$ not only increases the Al-OH-Al group, but also weakens the ability of Al^{3+} competing with Fe^{3+} for PO_4^{3-}. There is an absorption peak near 595 cm^{-1} in the three samples, which corresponds to the bending vibration of Fe-OH [36]. PFPS

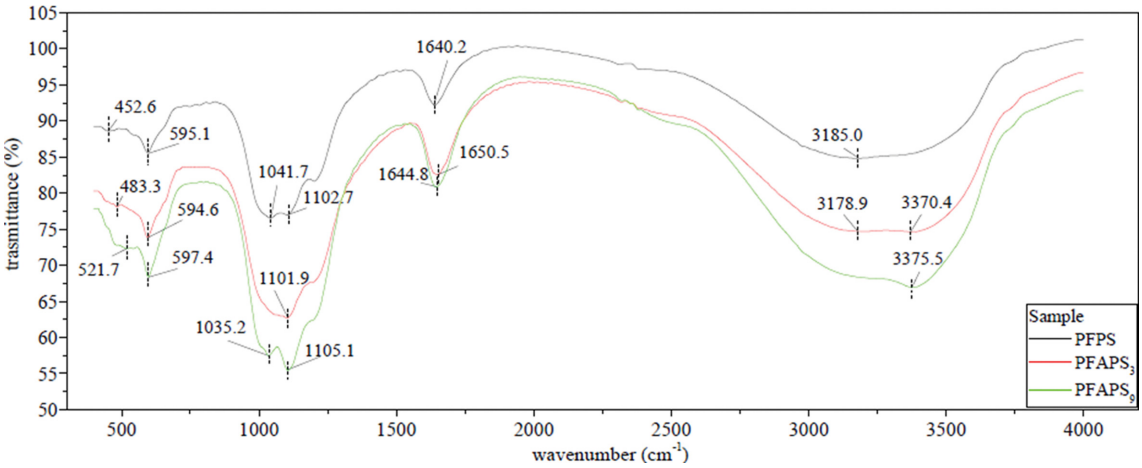

Fig. 4. FTIR results of the powder samples of PFPS, $PFAPS_3$ and $PFAPS_9$.

has an absorption peak near 452.6 cm^{-1}, which corresponds to the Fe-O group, while $PFAPS_3$ and $PFAPS_9$ have absorption peaks at 483.3 cm^{-1} and 521.7 cm^{-1}, respectively, which can be attributed to the superposition of the absorption peaks of Fe-O and Al-OH [36]. In conclusion, there are chemical bonds formed by the combination between Al^{3+}, Fe^{3+} and H_2O, OH^-, PO_4^{3-} in PFAPS, which is consistent with the MD results.

3. Flocculation Performance of PFAPS

3-1. Effect of Al/Fe

The decolorization rate of RTB and DY wastewater treated by PFAPS samples with different ratios of Al/Fe and the pH value of supernatant after treatment are shown in Fig. 5. With the increase of Al/Fe, the decolorization rate of PFAPS first increases and then decreases. And the highest decolorization rate is got by $PFAPS_3$ with Al/Fe=0.15. Specifically, for RTB, when the dosage is 32 mg/L, the decolorization rate raises from 85.2% of PFPS to 96.8% of $PFAPS_3$ with Al/Fe=0.15, then reduce to 95.8% of $FPSiS_4$ with Al/Fe=0.2; for the DY wastewater, when the dosage is 17.5 mg/L, the decolorization rate raises from 86.2% of PFPS to 97.6% of $PFAPS_3$ with Al/Fe=0.15, then reduce to 96.0% of $FPSiS_4$ with Al/Fe=0.2. This is because that the increase of Al/Fe can improve the number of positively charged metal polymer in flocculant samples, which enhances their ability of compressing electric double layer and electric neutralization, resulting in the improvement of the flocculation performance. However, the added Al^{3+} will compete with Fe^{3+} for PO_4^{3-} and OH^-. On the one hand, the decrease of OH^-/3(Fe+Al) can reduce the polymerization of Fe-polymer, which is not conducive to their ability of adsorption bridging and net sweeping; on the other hand, weakening the enhancement of PO_4^{3-} on the stability of the Fe-polymer will increase the content of uncharged precipitates. These two aspects have an adverse effect on the flocculation performance of PFAPS. The above factors lead to that the flocculation effect of PFAPS increases first and then decreases, with the increase of Al/Fe.

For the RTB wastewater, the pH value of the supernatant changes little first and then decreases significantly with the addition of flocculant. This is because when the dosage of flocculant is small, most of the polymers in the sample are combined with the pollutants in the simulated wastewater. When the dosage of flocculant is large, after combining with the pollutants, the remaining polymer can be hydrolyzed in the simulation wastewater. Moreover, the increase of Al/Fe improves the concentration of metal polymer in

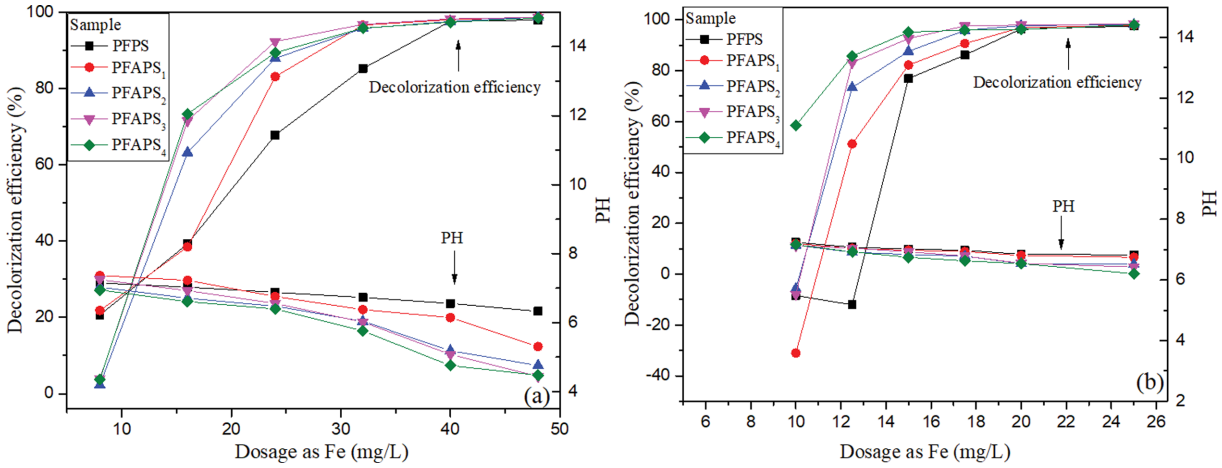

Fig. 5. Decolorization efficiency of PFAPS samples with different Al/Fe ratios on RTB (a) and DY (b) wastewater and pH of their supernatant.

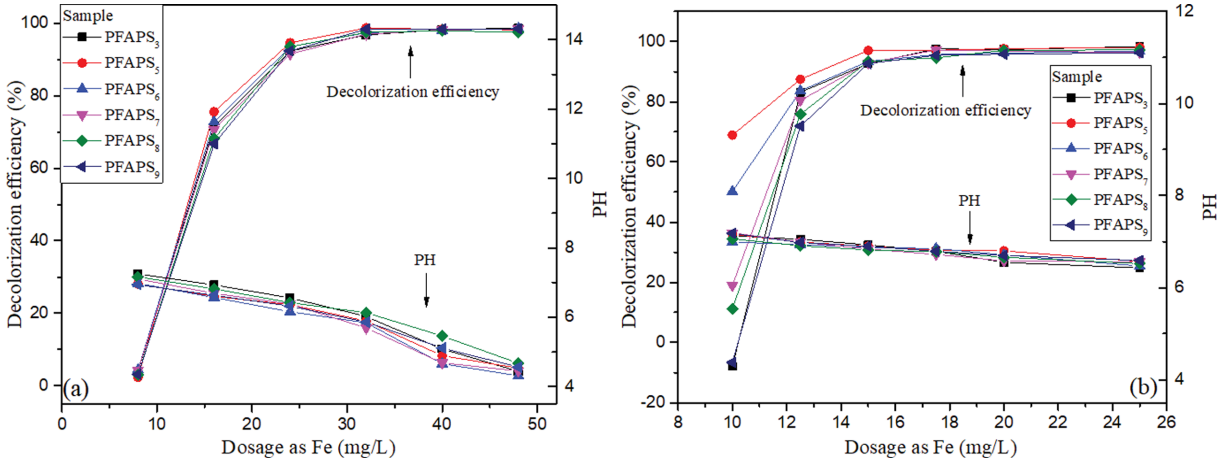

Fig. 6. Decolorization efficiency of PFAPS samples with different OH^-/Fe on RTB (a) and DY (b) wastewater and pH of their supernatant.

Table 4. Residual ion in supernatant treated by $PFAPS_{1-9}$

No	RTB simulated dye wastewater			DY simulated dye wastewater		
	Al^{3+} (mg/L)	PO_4^{3-} (mg/L)	P (mg/L)	Al^{3+} (mg/L)	PO_4^{3-} (mg/L)	P (mg/L)
$PFAPS_1$	0.34	0.9	0.28	0.04	0.6	0.19
$PFAPS_2$	1.05	0.6	0.19	0.02	0.5	0.16
$PFAPS_3$	1.85	0.3	0.09	0.04	0.5	0.16
$PFAPS_4$	2.3	0.2	0.06	0.06	0.3	0.09
$PFAPS_5$	1.9	0.4	0.13	0.03	0.3	0.09
$PFAPS_6$	1.95	0.6	0.19	0.03	0.5	0.16
$PFAPS_7$	1.9	0.5	0.16	0.05	0.7	0.22
$PFAPS_8$	1.72	0.8	0.25	0.04	0.6	0.19
$PFAPS_9$	0.15	0.8	0.25	0.04	0.5	0.16

the sample which improves their hydrolysis ability. So that the increase of Al/Fe expands the decrease of pH increases. For the DY wastewater, the pH value of supernatant changes little with the dosage of flocculant, which can be due to adsorption of negatively charged DY and its flocs on positively charged polymers.

3-2. Effect of OH^-/Fe

The decolorization rate of RTB and DY wastewater treated by PFAPS samples with different ratios of OH^-/Fe and the pH value of supernatant after treatment are shown in Fig. 6. With the increase of OH^-/Fe, the decolorization rate of PFAPS increases firstly and then decreases. And the highest decolorization rate is got by $PFAPS_5$ with OH^-/Fe=0.025. Specifically, for the RTB wastewater, when the dosage is 16 mg/L, the decolorization rate raises from 71.5% of $PFAPS_3$ with OH^-/Fe=0 to 75.6% of $PFAPS_5$ with OH^-/Fe=0.025, then reduce to 66.7% of $FPSiS_9$ with OH^-/Fe=0.3; for the DY wastewater, when the dosage is 12.5 mg/L, the decolorization rate raises from 83.2% of $PFAPS_3$ with OH^-/Fe=0 to 87.5% of $PFAPS_3$ with OH^-/Fe=0.025, then reduce to 71.9% of $FPSiS_9$ with OH^-/Fe=0.3. This is because that the increase of OH^-/Fe improve the active component Fe_b in PFAPS samples firstly, then further increase of OH^-/Fe will make Fe_b turn into Fe_c which has limited flocculation. The polymerization of Al-polymer is also promoted by the increase of OH^-/Fe. Because of the excellent stability of Al polymer, its flocculation ability is maintained or even improved. However, it cannot change the trend of flocculation effect decreasing.

For the RTB wastewater, the pH value of supernatant still changes little firstly and then decreases significantly with the increase of flocculant dosage. For the DY wastewater, the pH of the supernatant also changes little with the amount of flocculant.

4. Residual PO_4^{3-} and Al^{3+} in Supernatant

The residual PO_4^{3-} and Al^{3+} of DY and RTB simulated dye wastewater supernatant treated by $PFAPS_{1-9}$ in experimental maximum dose are shown in Table 4. The results show that concentration of Al^{3+} and PO_4^{3-} in all supernatants can meet the emission standard [41,42].

CONCLUSION

MD simulation results show Fe^{3+} and Al^{3+} form Fe-monomer and Al-monomer by combining with six oxygen atoms from H_2O or anion, which is consistent with FTIR results. And then these monomers form polymers through the bridging of various anions. Although the binding mode is similar, XRD results show that PFAPS and PFPS are amorphous. Although the addition of Al^{3+} can increase the number of positively charged metal polymer in PFAPS, it will also compete with Fe^{3+} for OH^- and PO_4^{3-}, which affect the polymerization and stability of Fe polymer negatively, resulting in the flocculation performance of PFAPS increases first and then decreases slightly with the increase of Al/Fe. A suitable increase of OH^-/Fe can promote the formation of active components Fe_b. While the continuous increase of OH^-/Fe can make Fe_b turn into Fe_c which has limited flocculation. The increase of OH^-/Fe can also promote the polymerization of Al-polymer. Due to the excellent stability of Al-polymer, its flocculation ability is maintained or even improved. However, it cannot change the trend of flocculation effect decreasing.

ACKNOWLEDGEMENT

This work is funded by The National Key Research and Development Program of China (Project No. 2017YFC0210203-4).

SUPPORTING INFORMATION

Additional information as noted in the text. This information is available via the Internet at http://www.springer.com/chemistry/journal/11814.

REFERENCES

1. D. Masseroni, G. Ercolani, E. A. Chiaradia and C. Gandolfi, *Hydrol. Res.*, **50**(5), 1293 (2019).
2. J. Yao, G. Wang, B. Xue, G. Xie and Y. Peng, *Hydrol. Res.*, **51**(5), 854 (2020).
3. S. S. Mohtar, T. N. Z. T. M. Busu, A. M. M. Noor, N. Shaari, N. A. Yusoff, M. A. C. Yunus and H. Mat, *Clean Technol. Environ.*, **19**(1), 191 (2017).
4. Z. Song and N. Ren, *J. Environ. Sci.*, **20**(2), 129 (2008).
5. Y. Sun, C. Zhu, H. Zheng, W. Sun, Y. Xu, X. Xiao, Z. You and C. Liu, *Chem. Eng. Res. Des.*, **119**, 23 (2017).
6. H. Rong, B. Gao, R. Li, Y. Wang, Q. Yue and Q. Li, *Chem. Eng. J.*, **243**, 169 (2014).

7. X. Niu, X. Li, J. Zhao, Y. Ren and Y. Yang, *J. Environ. Sci.*, **23**(7), 1122 (2011).
8. H. Eslami, A. Esmaeili, M. H. Ehrampoush, A. A. Ebrahimi, M. Taghavi and R Khosravi, *J. Water Process Eng.*, **36**, 101342 (2020).
9. K. J. Choi, S. G. Kim and S. H. Kim, *J. Hazard. Mater.*, **151**(1), 38 (2008).
10. Y. H. Shen and B. A. Dempsey, *Environ. Int.*, **24**(8), 899 (1998).
11. N. Parthasarathy and J. Buffle, *Water Res.*, **19**(1), 25 (1985).
12. T. Sun, C. H. Sun, G. L. Zhu, X. J. Miao, C. C. Wu, S. B. Lv and W. J. Li, *Desalination*, **268**(1-3), 270 (2011).
13. Z. P. Xing and D. Z. Sun, *J. Hazard. Mater.*, **168**(2-3), 1264 (2009).
14. R. J. Ward, Y. Zhang and R. R. Crichton, *J. Inorg. Biochem.*, **87**(1-2), 9 (2001).
15. M. Murali, P. Athif, P. Suganthi, A. S. Bukharia, H. E. S. Mohamed, H. Basu and R. K. Singhal, *Environ. Toxicol. Phar.*, **59**, 74 (2018).
16. T. P. Flaten, *Environ. Geochem. Hlth.*, **12**, 152 (1990).
17. A. Zouboulis, P. Moussas and F. Vasilakou, *J. Hazard. Mater.*, **155**(3), 459 (2008).
18. D. Li, Y. Kang, J. Li and X. Wang, *Korean J. Chem. Eng.*, **36**(9), 1499 (2019).
19. M. Fan, S. Sung, R. C. Brown, T. D. Wheelock and F. C. Laabs, *J. Environ. Eng-Asce.*, **128**(6), 483 (2002).
20. F. M. Mohamed and K. A. Alfalous, *Egypt. J. Aquat. Res.*, **46**(2), 131 (2020).
21. T. Sun, L. Liu, L. Wan and Y. Zhang, *Chem. Eng. J.*, **163**(1-2), 48 (2010).
22. C. Sun, Q. Yue, B. Gao, R. Mu, J. Liu, Y. Zhan, Z. Yang and W. Xu, *Desalination*, **281**, 243 (2011).
23. T. Sun, C. Sun, G. Zhu, X. Miao, C. Wu, S. Lv and W. Li, *Desalination*, **268**(1-3), 270 (2011).
24. M. J. Abraham, T. Murtola, R. Schulz, S. Páll, J. C. Smith, B. Hess and E. Lindal, *SoftwareX*, **1-2**, 19 (2015).
25. T. Lu and F. Chen, *J. Comput. Chem.*, **33**(5), 580 (2012).
26. J. Wang, R. M. Wolf, J. W. Caldwell, P. A. Kollman and D. A. Case, *J. Comput. Chem.*, **25**(9), 1157 (2004).
27. P. Li, L. F. Song and K. M. Merz, *J. Phys. Chem. B*, **119**(3), 883 (2014).
28. L. Martínez, R. Andrade, E. G. Birgin and J. M. Martínez, *J. Comput. Chem.*, **30**(13), 2157 (2009).
29. GB/T 14591-2016, Water treatment chemicals-Poly ferric sulfate, Chinese standard (2016).
30. A. Zouboulis, P. Moussas and F. Vasilakou, *J. Hazard. Mater.*, **155**(3), 459 (2008).
31. B. Yang, S. Jiang, C. Zhang, G. Zhao, M. Wu, N. Xiao and P. Su, *Chemosphere*, **283**, 131216 (2021).
32. N. Yang, H. Xiao, K. Pi, J. Fang, S. Liu, Y. Chen, Y. Shi, H. Zhang, A. R. Gerson and D. Liu, *Chemosphere*, **269**, 129403 (2021).
33. P. Ke, Z. Liu and L. Li, *Int. J. Min. Met. Mater.*, **25**(10), 1217 (2018).
34. J. Sun, *Structural features and evolution mechanisms of two new Al_{30} and Al_{13} species*, Inner Mongolia: Inner Mongolia University (2019).
35. R. Li, C. He and Y. He, *Chem. Eng. J.*, **223**, 869 (2013).
36. Y. Sun, C. Zhu, H. Zheng, W. Sun, Y. Xu, X. Xiao, Z. You and C. Liu, *Chem. Eng. Res. Des.*, **119**, 23 (2017).
37. W. Chen, B. Li, Q. Li and J. Tian, *Constr. Build. Mater.*, **124**, 1019 (2016).
38. A. Zouboulis, P. Moussas and F. Vasilakou, *J. Hazard Mater.*, **155**(3), 459 (2007).
39. W. Chen, H. Zheng, H. Teng, Y. Wang, Y. Zhang, C. Zhao and Y. Liao, *PLOS ONE*, **10**(9), e0137116 (2015).
40. Y. Fang, X. Zhao and X. Zhang, *Ind. Saf. Environ. Prot.*, **33**(10), 22 (2007).
41. DB12/356-2018, Integrated wastewater discharge standard, Chinese standard (2018).
42. GB/T 21900-2008, Emission standard of pollutants for electroplating, Chinese standard (2008).

Supporting Information

Polymerization mechanism of polyferric aluminum phosphatic sulfate (PFAPS) and its flocculation effect on simulated dye wastewater

Shaopu Li and Yong Kang †

School of Chemical Engineering and Technology, Tianjin University, Tianjin 300350, China
(*Received 25 September 2021 • Revised 29 November 2021 • Accepted 2 December 2021*)

Different kinds of Fe-monomers and Al-monomers in PFPS, $PFAPS_3$ and $PFAPS_8$ system are shown in Fig. S1 and Fig. S2, respectively. Typical micro polymers in PFPS, $bPFAPS_3$ and $PFAPS_8$ system are shown in Fig. S3.

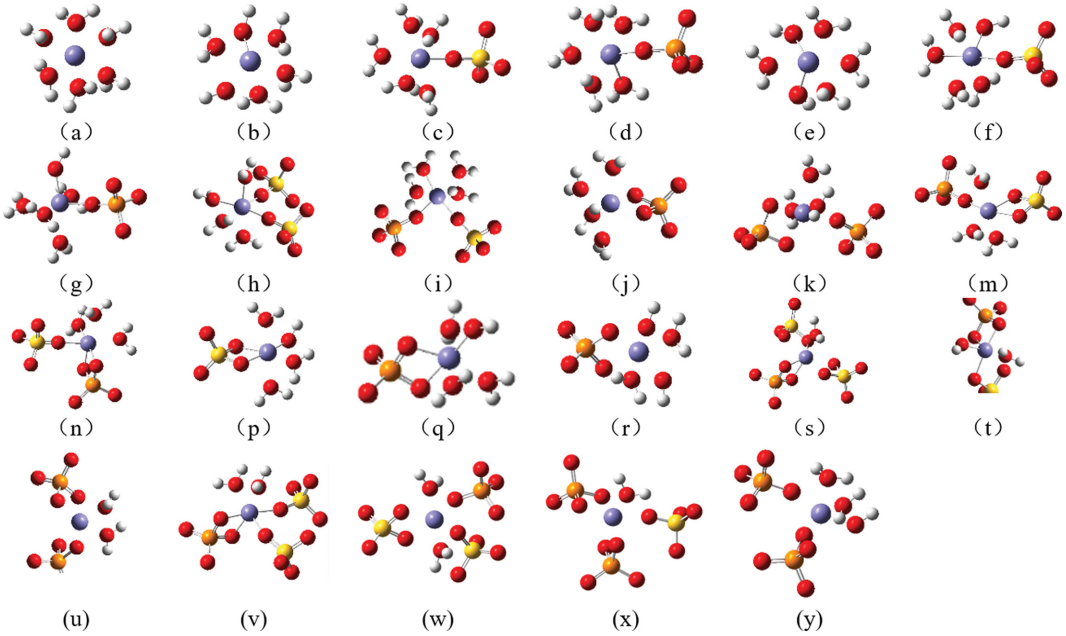

Fig. S1. Fe monomers in the simulation systems of PFPS, $PFAPS_3$ and $PFAPS_8$ (Red: O, White: H, Yellow: S, Blue: Fe, Orange: P).

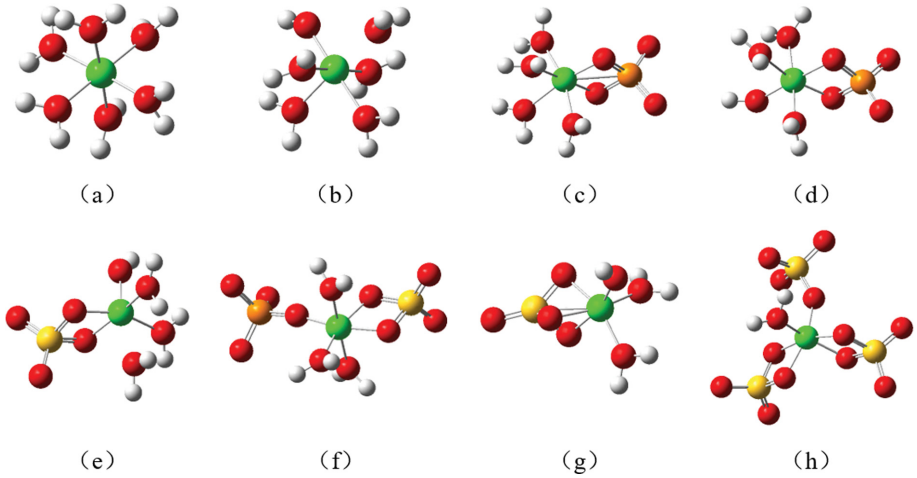

Fig S2. Al monomer in the simulation systems of PFPS, $PFAPS_3$ and $PFAPS_8$ (Red: O, White: H, Yellow: S, Orange: P, Green: Al).

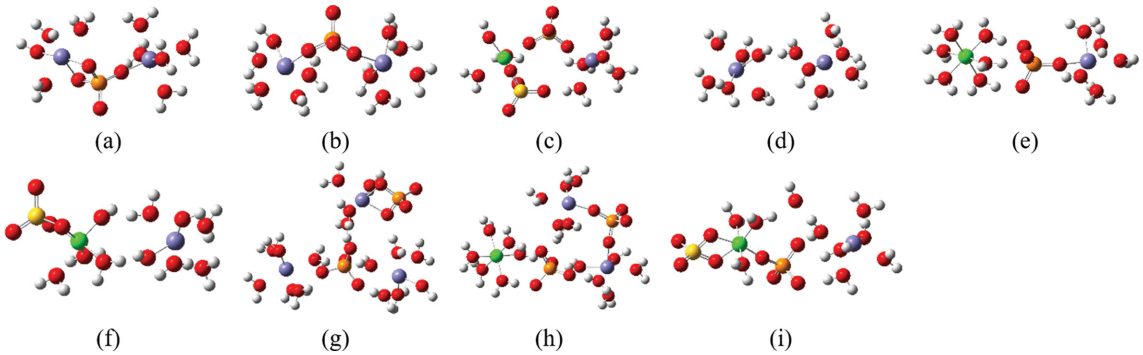

Fig. S3. Typical micro polymer in the simulation systems of PFPS, $PFAPS_3$ and $PFAPS_8$ (Red: O, White: H, Yellow: S, Blue: Fe, Gray: Si, Orange: P, Green: Al).